Efflux of Iron from the Cerebrospinal Fluid to the Blood at the Blood-CSF Barrier: Effect of Manganese Exposure

XUEQIAN WANG,*,[1] G. JANE LI,† AND WEI ZHENG*,[2]

*School of Health Sciences, Purdue University, West Lafayette, Indiana 47907; and †Beijing Municipal Health Bureau, Beijing Municipal Centers for Disease Prevention and Control, Beijing, China 100080

The blood-cerebrospinal fluid (CSF) barrier (BCB) resides within the choroid plexus, with the apical side facing the CSF and the basolateral side towards the blood. Previous studies demonstrate that manganese (Mn) exposure in rats disrupts iron (Fe) homeostasis in the blood and CSF. The present study used a primary culture of rat choroidal epithelial cells grown in the two-chamber Transwell system to investigate the transepithelial transport of Fe across the BCB. Free, unbound Fe as [^{59}Fe] was added to the donor chamber and the radioactivity in the acceptor chamber was quantified to determine the direction of Fe fluxes. Under the normal condition, the [^{59}Fe] efflux (from the CSF to the blood) was 128% higher than that of the influx ($P < 0.01$). Mn exposure significantly increased the efflux rate of [^{59}Fe] ($P < 0.01$) and the effect was inhibited when the cells were pre-incubated with the antibody against divalent metal transport 1 (DMT1). Moreover, when the siRNA knocked down the cellular DMT1 expression, the elevated Fe uptake caused by Mn exposure in the choroidal epithelial Z310 cells was completely abolished, indicating that Mn may facilitate Fe efflux via a DMT1-mediated transport mechanism. *In vivo* subchronic exposure to Mn in rats reduced Fe clearance from the CSF, as demonstrated by the ventriculo-cisternal brain perfusion, along with up-regulated mRNAs encoding DMT1 and transferrin receptor (TfR) in the same animals. Taken together, these data suggest that free Fe appears to be favorably transported from the CSF toward the blood by DMT1 and this process can be facilitated by Mn exposure. Enhanced TfR-mediated influx of Fe from the blood and ferroportin-mediated expelling Fe toward the CSF may compromise DMT1-mediated efflux, leading to an increased Fe concentration in the CSF as seen in Mn-exposed animals. Exp Biol Med 233:1561–1571, 2008

Key words: iron; manganese; choroid plexus; blood-CSF barrier; *in vitro* Transwell model; ventriculo-cisternal perfusion

Introduction

The chemical homeostasis of brain extracellular fluid is maintained by two major brain barrier systems, i.e., the blood-brain barrier (BBB) that separates the blood circulation from brain interstitial fluid and the blood-cerebrospinal fluid barrier (BCB) that separates the blood from the cerebrospinal fluid (CSF). Both barriers selectively allow essential nutrients, metal ions and drug molecules to enter the brain parenchyma. In addition, they remove brain metabolites or unwanted materials from brain extracellular fluid. The choroid plexus, a highly vascularized tissue, constitutes the BCB, with the basolateral side of the choroidal epithelium facing the blood and the apical microvilli border directly contacting the CSF. Cumulative evidence has suggested that the choroid plexus plays an important role in transporting materials including metals such as iron (Fe) between the blood and the CSF in both directions (1).

Regulation of iron (Fe) homeostasis in the BCB involves multiple steps that control Fe transport, storage and regulation. Excess Fe in cells can produce reactive oxygen species (ROS) through Fenton reaction. In the central nervous system (CNS), this may serve as a common mechanism contributing to various neurodegenerative diseases such as Parkinson's disease, Alzheimer's disease, amyotrophic lateral sclerosis, prion disease, Friedreich's ataxia and cataracts (2–5). Major proteins involved in Fe metabolism include divalent metal transporter-1 (DMT1), ferroportin or metal transporter protein-1 (MTP1), transferrin receptor (TfR), iron regulatory protein (IRP)-1 and –2 (IRP1 and IRP2), heavy and light chain ferritin, p97, as well as lactoferrin (6, 7). Coordinated function of these proteins

This study was partially supported by NIH/National Institute of Environmental Health Science Grants ES08146 and ES013118, and Lilly Research Foundation.

[1] Current address: NIH/NIEHS, Research Triangle Park, NC 27709.

[2] To whom correspondence should be addressed at School of Health Sciences, Purdue University, 550 Stadium Mall Drive, Room 1163D, West Lafayette, IN 47907. E-mail: wzheng@purdue.edu

Received March 23, 2008.
Accepted July 29, 2008.

DOI: 10.3181/0803-RM-104
1535-3702/08/23312-1561$15.00

at brain barriers keeps Fe influx and efflux in balance. However, the exact mechanisms by which brain barriers regulate Fe transport are poorly understood.

Previous studies from this group have shown that subchronic manganese (Mn) exposure in rats decreases blood Fe concentrations while it increases Fe levels in the CSF (8, 9), suggesting a Mn-facilitated increase of Fe influx from the systemic circulation to the CSF. Our earlier studies also demonstrate that a functional change in the conformation of IRP1 may up-regulate the expression of TfR for Fe transport by brain barriers and down-regulate the expression of ferritin for Fe storage (10). At the molecular level, it occurs through an increased binding activity between IRP1 and the iron responsive element (IRE) located at 3′ mRNA transcripts of TfR and DMT1. The active center of IRP1 contains a [4Fe-4S] cluster, with one labile Fe whose presence or absence in the cluster determines the IRP1 either as an iron regulatory protein or as an enzyme participating in cellular energy production. Toxic metal Mn may replace the labile Fe in IRP1 structure so that IRP1 binds with a high affinity to IRE-containing TfR or DMT1 mRNAs, stabilizes the expression of these two Fe transporters, and increases intracellular levels of Fe (11, 12).

Transferrin (Tf)-bound Fe and non-Tf-bound Fe are two primary species of Fe in the CSF and interstitial fluid (13, 14). Some 35–60% of free, unbound [^{59}Fe] could be transported into rat brain through a non-Tf route (15, 16), while the rate of free [^{59}Fe] transported into the CSF is 53% of Tf-bound [^{59}Fe] measured through the use of a brain perfusion technique, suggesting an equally important role of these two forms in Fe delivery in the CNS (16–19). Tf-bound Fe binds with a high affinity to TfR; the complex then enters the cytoplasm by receptor-mediated endocytosis (20, 21). The dissociation of Fe from transferrin occurs in low-pH endosomes, where ferroportin may participate in exporting Fe from the endosome to cytosol (17). Our recent work has demonstrated that Mn exposure induces subcellular relocation of ferroportin, rendering it highly concentrated in the microvilli of choroidal apical epithelia (22). However, the exact role of the choroid plexus in mediating Fe transport with regards to the direction of Fe fluxes across the BCB, i.e., from the blood to CSF or vice versa from the CSF to blood, was unknown. Furthermore, to what extent DMT1, TfR, and/or ferroportin may contribute to elevated Fe levels in the CSF following Mn chronic exposure remained elusive.

The purposes of this study were 1) to demonstrate the distribution of DMT1 and TfR in a two-chamber Transwell transport system and to determine the direction of free Fe transport in the *in vitro* BCB model under normal conditions; 2) to explore whether Mn exposure altered Fe transport across the BCB; 3) to study Fe uptake in choroidal epithelial cells after knocking down DMT1 by RNA interference (RNAi) technique; and 4) to investigate whether subchronic Mn exposure in rats affected Fe clearance from the CSF by a ventriculo-cisternal perfusion technique.

Materials and Methods

Materials. Chemicals and reagents used in primary cell culture were purchased from the following sources: Hank's balanced salt solution (HBSS), fetal bovine serum (FBS), Dulbecco's modified Eagle's medium (DMEM), and antibiotic-antimycin solution (100×) from Gibco (Grand Island, NY), epidermal growth factor (EGF) from Roche Applied Science (Indianapolis, IN), pronase and protease from Calbiochem (La Jolla, CA), and bafilomycin A1, collagen and rat apo-transferrin from Sigma (St. Louis, MO). [^{59}Fe] in 0.5 M HCL was obtained from PerkinElmer (Waltham, MA), [^{14}C]sucrose from Moravek Biochemicals (Brea, CA), and Eco-lite-(+) scintillation cocktail from MP Biomedicals (Irvine, CA). Collagen-coated Transwell-COL inserts were purchased from Costar (Cambridge, MA). Rabbit anti-rat DMT1 antibody was obtained from Alpha Diagnostic (San Antonio, CA), mouse anti-human TfR antibody from ZYMED Laboratories (South San Francisco, CA), and Alexa-labeled secondary antibodies from Molecular Probes (Eugene, OR). All reagents were of analytical grade, HPLC grade or the best available pharmaceutical grade.

Culture of Primary Rat Choroidal Epithelial Cells and Immortalized Z310 Cells. The method for establishing and maintaining rat choroidal epithelial cell culture has been described in details in our previous publications (23, 24). Male Sprague-Dawley rats (150–174 g, 4–6 weeks old) were purchased from Harlan (Indianapolis, IN). Choroid plexuses from both hemispheres were dissected and digested in HBSS containing 0.2% pronase at 37°C for 6 min. The digested cells were washed twice with HBSS and resuspended in the DMEM growth medium containing 10% FBS, 100 units/ml penicillin, 100 μg/ml streptomycin, 0.25 μg/ml amphotericin, 100 μg/ml gentamycin and 10 ng/ml EGF. A 20-gauge needle was used to pass cells through for 13–14 times to ensure good cell separation. The cells stained with 0.4% Trypan blue were counted under the light microscope before they were plated in 35-mm Petri dishes (pre-coated with 0.01% collagen) at the density of 2–3 $\times$ 10^5/ml. The cultured cells were maintained at 37°C with 95% air–5% CO_2 in a humidified incubator without disturbance for at least 48 hours. The growth medium was replaced 3 days after the initial seeding and every 2 days thereafter. All procedures were conducted in the controlled-sterile conditions to avoid cell contamination. The study was conducted in compliance with animal rights and approved by the Animal Care and Use Committee of Purdue University.

Z310 cells were originally derived from rat choroid plexus epithelia and the detailed procedure for culture and maintenance can be found in a previous publication (25). In short, the cells were grown in DMEM supplemented with

10% FBS, 100 units/ml penicillin, 100 μg/ml streptomycin, and 10 μg/ml of gentamycin in 100 mm Petri plates in a humidified incubator with 95% air–5% CO_2 at 37°C. Trypsin-EDTA was used to digest cells during subculture and Z310 cells were passaged twice a week.

Culture on Two-Chamber Transwell System. The culture system mimicking the blood-CSF barrier was well established in this laboratory (23, 26). After cultured in dishes for 8–10 days, a typical polygonal morphology of choroidal epithelial cells could be found dominant with no visible spaces between cells. Cells were then transferred to the two-chamber Transwell culture system. The device was composed of inner and outer chambers. The inner chamber has the diameter of 12 mm and hangs in an outer chamber. The inner chamber membrane is kept about 3 mm off the bottom of the outer chamber. The permeable membrane between the two chambers was made of polytetrafluoroethylene (PTFE) with the pore size of 0.4 μm, which was pre-coated with laminin (14 μg/ml) to enhance cell attachment. The Transwell membrane was transparent when wet, allowing cells to be visualized during the culture. An overnight period for initial equilibrium across the Transwell membrane was used to improve cell attachment by adding medium to the 12-well plate and the Transwell insert prior to initial seeding. An aliquot of 0.8 ml cell suspension (2×10^5/ml for initial seeding) was added to the inner chamber and 1.2 ml of medium was added to the outer chamber. When the cell grew to the confluence, the level of medium surface in the inner chamber was about 2 mm higher than that of the outer chamber. The transepithelial electrical resistance (TEER), an indicator of the tightness of the barrier, was used to track the formation of cell monolayer tight barrier between the inner and outer chambers. The TEER value was measured every other day by an Epithelial Volt-Ohmmeter (EVOM, World Precision Instruments, Sarasota, FL). The same two-chamber system without cells was used as the black and its background value was deducted from the measured TEER.

Confocal Immunofluorescence Microscopy Studies of DMT1 and TfR in Primary Choroidal Epithelial Cells. The inner chamber was taken out and placed in a small Petri dish. Cells were fixed with 3% paraformaldehyde/0.25% glutaraldehyde in PBS and permeabilized with 0.5% Triton X-100, followed by blocking with 1% BSA in PBS. The cells were then incubated with rabbit anti-DMT1 (0.2 μg/μl) or mouse anti-TfR antibody (1:100) in 1% BSA at 37°C for 60 min, followed by probing with Flour Alexa-488-conjugated secondary antibody (1:500) in 1% BSA at 37°C for 60 min. Finally, propidium iodide (1 μg/ml) was used for nuclear staining. Negative controls were established by using only secondary antibody to reflect nonspecific staining on the background. Primary cells growing on the inner chamber were observed under a confocal microscope and Z-series pictures were taken to show the vertical view.

***In Vitro* Iron Transport Study.** The culture with confluent cells growing on the Transwell device was used to investigate the transepithelial transport of Fe. Cells were exposed to 100 μM $MnCl_2$ in serum-free medium for 24 hours at 37°C. The Fe transport as [^{59}Fe] was assessed separately. In some studies, the antibody against DMT1 was added to the inner chamber and the incubation continued for 2 hours at 37°C to block DMT1-mediated Fe transport. [^{14}C]sucrose was used as a space marker to determine the paracellular leakage. The following specific procedures were taken:

(1) [^{59}Fe] transport. An aliquot (8.5 μl) of [^{59}Fe] in 0.5 M HCl was mixed with 150 μl of [^{14}C]sucrose (specific activity: 495 mmCi/mmol) to a final concentration of 4.8 mM with 14.1 μCi/ml [^{59}Fe] and 1 μM with 0.5 μCi/ml [^{14}C]sucrose in serum-free medium. All the transport procedures were conducted on the heat block maintaining at 37°C. For the influx study, [^{59}Fe]-containing medium was added to the outer chamber (donor) and an aliquot (10 μl) of medium was taken as the initial donor radioactivity. A series of time points (0, 5, 10, 20, 30 min, 1, 2, 4, 6, 12 to 24 hour) were set for sample collection. At each time point, 10 μl of medium was taken from the inner (receiver) chamber and replaced with an equal volume of fresh serum-free medium. The efflux study was conducted in the same way except that the inner chamber was the donor and the outer chamber was the receiver.

All the samples were counted by an auto-Gamma 5000 Series Gamma Counter (Packard Instrument Company, counting efficiency for [^{59}Fe]: 3.98%). To count [^{14}C]sucrose, the samples were mixed with Eco-lite cocktail and counted on a Packard Tri-Carb 2900 TR Liquid Scintillation Analyzer (counting efficiency for [^{14}C]: 94%).

(2) Retention of Fe in cells grown on two-chamber Transwells. After the final wash, each membrane on the bottom of the inner chamber was removed. Cell lysis solution (0.5 ml) containing 0.2 M NaOH and 1% SDS was added to solubilize cells for 30 min at room temperature. Cell lysates were neutralized by equal-molar HCl to the pH 7. The half of lysates were saved for protein assay by the Bicinchoninic Acid (BCA) method and the other half were used for radioactivity counting. The cellular Fe retention was assessed by calculating V_D (the volume of distribution), which was the ratio of radioactivity in cell lysates (dpm/g) to the radioactivity to medium (dpm/ml).

(3) Data analysis. The radioactivities for [^{59}Fe] and [^{14}C]sucrose obtained from all time points were plotted as the function of treatment time. To determine the permeability coefficient across the *in vitro* Transwell cell membrane, the linear portion on the time-dependent curve was used for linear regression analysis using Prism linear curve-fit equation (Prism 3.0, GraphPad Software Inc., San Diego). The slope of each linear equation was used to calculate the permeability coefficient (P_E) of the epithelial barrier based on the following equation,

$$1/P_E = 1/P_T - 1/P_B,$$

where P_T is the total permeability coefficient including cells, membrane and coating materials; P_B is the blank permeability coefficient accounting for the membrane and the coating. P_T and P_B can be calculated as apparent permeability P_A from the equation below,

$$P_A = (dC_R/dt) \cdot V_R/(A \times C_D),$$

where P_A is apparent permeability and dC_R/dt the change of radioisotope activity in the receiver chamber over time. V_R, A, and C_D are constant parameters for culture well: V_R, the volume in the receiver chamber (0.8 ml); A, the surface area of transport membrane (1 cm^2); C_D, the initial counting in the donor chamber (dpm/ml).

Fe Uptake in Z310 Cells Following DMT1 Knockdown. Candidate sequences for DMT1 knockdown were self-designed by using the Ambion website. Sequence 1: 5′-AAT CCT CCT CAG GAA TGG GGA CCT GTC TC-3′ as forward; 5′-AAT CCC CAT TCC TGA GGA GGA CCT GTC TC-3′ as reverse. Sequence 2: 5′-AAC TCC TCA GGA ATG GGG ATT CCT GTC TC-3′ as forward; 5′-AAA ATC CCC ATT CCT GAG GAG CCT GTC TC-3′ as reverse. Silencer siRNA was constructed following the manufacturer's guide (Silencer siRNA Construction Kit, Ambion). Synthesized siRNAs were further assessed by gel electrophoresis on 2% agarose gel and visualized under UV transilluminator. The siRNA should migrate as a 21–22 bp band that runs slightly behind the bromophenol blue dye front. A second, less intense band may be observed running behind the primary siRNA band. Transfection reagent siPORT amine was found to work best in our Z310 cell line after a series of screening. Transfection conditions were optimized according to the following variables: initial seeding density, volume of transfection agent, duration of transfection, siRNA quantity.

Cells were seeded at an initial density of 5×10^4/well in 65-mm Petri dish growing in the normal medium. After 24 hours growth, the RNA/transfection complexes were prepared by the following steps: 7.5 μl of Amine was diluted in 125 μl of OPTI-MEM I reduced medium and incubated for 10 min at room temperature; an appropriate amount of siRNA was diluted in OPTI-MEM I reduced medium for a final concentration of 30 nM per dish; siRNA and transfection reagent were mixed and incubated at room temperature for 10 minutes. Cell medium was replaced with OPTI-MEM I reduced medium and the RNA/transfection reagent complexes were dispensed into culture dishes. At the end of transfection, cells were allowed to recover for at least 12 hours by replacing with normal complete medium. Gene knockdown was analyzed by real-time RT-PCR at different time points after transfection.

Cells were exposed to Mn at 100 μM for 24 hours. Cellular [^{59}Fe] uptake retention was conducted as described above. Half of the lysates were saved for protein assays by the Bicinchoninate BCA method and the other half were used for radioactivity counting. [^{59}Fe] uptake in Z310 cells was described as dpm/μg of protein.

***In Vivo* Subchronic Mn Exposure.** Male Sprague-Dawley rats were purchased from Harlan (Indianapolis, IN). At the time of use the rats were 7 weeks old weighing 220–250 g. Upon arrival, the rats were housed in a temperature-controlled room under a 12-hour light/12-hour dark cycle and allowed for acclimation for one week prior to experimentation. They had free access to pelleted rat chow (Basal Diet 5755, TestDiet, Richmond, IN) and distilled, deionized water. $MnCl_2$ dissolved in sterile saline was administrated by *i.p.* injection to rats at a dose of 6 mg of Mn/kg 5 days a week for 4 consecutive weeks. This exposure regimen has been used in our previous study (23). The daily equivalent volume of sterile saline was given to the animals in the control group. The study was conducted in compliance with animal rights and approved by Purdue Animal Care and Use Committee.

***In Situ* Ventriculo-Cisternal Perfusion.** Control and Mn-subchronically exposed rats were anesthetized by *i.p.* injection of ketamine/xylazine (75:10 mg/ml, 1 ml/kg) and immobilized in a stereotaxic device. A midline cutaneous incision was made from the forehead to neck and the top of skull was exposed. A hole was made in the skull by using a drill for insertion of guide cannula (Plastics One Inc., Roanoke, VA). The cannula was implanted into the lateral ventricle according to the following parameters on three scales: 0.8 mm posterior to the bregma, 1.4 mm lateral to the midline, and 4.0 mm vertical from the surface of skull (27, 28). An internal cannula connected to PE50 tubing was inserted into the guide cannula for lateral ventricle perfusion controlled by the pump-driven syringe filled with artificial CSF (aCSF). Pre-gassed aCSF containing 0.18 μCi/ml of [^{59}Fe] and 0.5 μCi/ml of [^{14}C] was delivered to the lateral ventricle at a rate of 28 μl/min controlled by a pump (Harvard Compact Infusion Pump, Model 975). A 26G butterfly needle was inserted at an appropriate angle into the cisterna magna for collection of the perfusion outflow. Cisternal outflow samples were collected over 10-minute intervals throughout the perfusion time (90 minutes). The CSF volume was determined by measuring its weight assuming that the CSF density was 1 g/ml. Additional anesthesia was given to rats in the hindquarter muscle as needed. Body temperature was maintained at 37°C using a heating pad during the perfusion. At the end of the perfusion, the animal was decapitated, the brain removed, and both lateral choroid plexus harvested. Samples were taken for liquid scintillation counting.

Quantitative Real-Time RT-PCR Analysis. Choroid plexus tissues were dissected from control and Mn-subchronically exposed rats. Levels of mRNA for DMT1, TfR and Tf were quantified using real-time RT-PCR as described previously (12). All real-time RT-PCR reactions were done in triplicate. The relative differences in gene expression between groups were expressed using cycle time (Ct) values. The Ct values of interested genes were first

normalized with that of GAPDH in the same sample; the relative differences between control and treatment groups were then calculated and expressed as relative increases by setting the control as 100%. Assuming that the Ct value is reflective of the initial starting copy and that there is 100% efficiency, a difference of one cycle is equivalent to a two-fold difference in starting copy.

Statistical Analysis. All data are expressed as mean ± SEM. Statistical analyses of the differences between groups were carried out by one-way ANOVA using SPSS 12.0 statistic package for Windows. Linear regression lines were plot with KaleidaGraph (version 3.6, Synergy software, Reading, PA). The differences between two means were considered significant if P values were equal or less than 0.05.

Results

The primary epithelial cells growing in the Transwell chamber culture system possesses the original morphology and polarity of choroid plexus. DMT1 stains were widely distributed in the cytoplasm of confluent cells grown as a monolayer on the semipermeable membrane (Fig. 1A, vertical view). TfR stains were primarily located in the cytosolic vesicles. The bright staining was localized around the nuclei, possibly organelle-associated (Fig. 1B). Formation of the barrier between two chambers was determined by the TEER, an indicator of the tightness of the barrier, which reached between 50–60 Ω-cm^2 in this study (Fig. 2), comparable to the values of 64.0 ± 1.66 Ω-cm^2 in the previous report (26).

Studies of Fe transport were conducted in the Transwell BCB model. Samples were collected over a 24-hour period. Since [^{14}C]sucrose reflects a non-specific leakage through the barrier, the permeability coefficient [^{59}Fe] was corrected by [^{14}C]sucrose and expressed as the ratio of [^{59}Fe] to [^{14}C]sucrose. Under normal conditions without Mn treatment, the free [^{59}Fe] efflux (from the CSF to the blood) in the BCB model was about 128% greater than that of the influx ($P < 0.01$, Fig. 3). Thus, it seems likely that the efflux of free Fe at the BCB is more favorable than the influx.

Exposure of culture cells to Mn significantly increased the efflux rate of [^{59}Fe] ($P < 0.01$, Fig. 4); the effect was specifically inhibited by pre-incubation of the cells with anti-DMT1 antibody. Thus, it appeared that the increased P_E of [^{59}Fe] was probably due to a DMT1-mediated mechanism, but not due to Mn-caused damage to the barrier structure. [^{59}Fe] retention in the cultured choroidal cells after the *in vitro* transport study was significantly higher in efflux studies than in the influx studies ($P < 0.05$, Fig. 5). Mn treatment, however, appeared to decrease the Fe retention in the cells within the same treatment group, although the magnitude of decrease did not reach the statistical significance.

We further used RNAi technique to knock down gene expression of DMT1 and to see how this may affect Fe uptake in the choroidal epithelial Z310 cells. Cells were transfected with either scrambled siRNA as negative control or siRNA sequence designed homologous to DMT1. The negative control was used to demonstrate that there was no non-specific toxicity caused by transfection reagent. Following targeted siRNA transfection, the gene expression of DMT1 reduced down to about 50% as compared to control (Fig. 6A). In the presence of Mn, [^{59}Fe] uptake in Z310 cells treated with the scrambled siRNA was significantly increased by 31% (Fig. 6B). Replacement of scrambled siRNA with DMT1 siRNA abolished the Mn effect. The cells without Mn treatment but with DMT1 knockdown took up even less Mn as compared to controls ($P < 0.05$) (Fig. 6B). Thus, the effect of Mn on free Fe uptake by the choroidal epithelial cells seemed to be DMT1-mediated.

By using an *in situ* ventriculo-cisternal brain perfusion technique, we investigated Fe clearance from the CSF following subchronic Mn exposure *in vivo*. [^{59}Fe] recovered from the cisternal effluent was expressed as the ratio of [^{59}Fe] concentration in the collected CSF effluent to that in the perfusate. Since the choroid plexus is the major tissue that removes materials present in the ventricular CSF, a higher recovery of [^{59}Fe] in the cisternal effluent suggests a less *in situ* uptake of [^{59}Fe] by the choroid plexus and thus a lower clearance from the CSF. In Mn-exposed animals, the [^{59}Fe] recovered in the cisternal effluent was greater than that of controls throughout the entire perfusion period (Fig. 7). Since the CSF secretion rate, measured by use of the space marker [^{14}C]sucrose, was not altered by subchronic Mn exposure (data not shown), the decreased Fe clearance from the CSF was apparently due to an impaired Fe uptake by the choroid plexus.

In the same animals, the upregulation of mRNAs encoding DMT1, TfR and Tf in the choroid plexus was observed (Fig. 8); the data were in a good agreement with our previous findings (9, 11, 12).

Discussion

Compared to *in vivo* studies using whole animals, the two-chamber Transwell culture system possesses the following advantages: 1) it serves as an alternative approach to the costly, time-consuming *in vivo* animal tests; 2) the polarized cells on the Transwell membrane can be used to study the orientation of toxicant transport across the BCB (24, 29); and 3) the system allows for complete control of the studied substances on either side of the barrier (30). By using this *in vitro* BCB model, we demonstrated that free Fe species was transported by the choroid plexus favorably from the CSF toward the blood. *In vitro* Mn exposure may facilitate this process. Yet, in Mn-exposed animals, Fe clearance from the CSF was in fact diminished.

DMT1-directed Fe transport primarily transports non-Tf-bound, divalent Fe ions, although other proteins, such as lactoferrin, melanotransferrin, p97 and ceruloplasmin, have

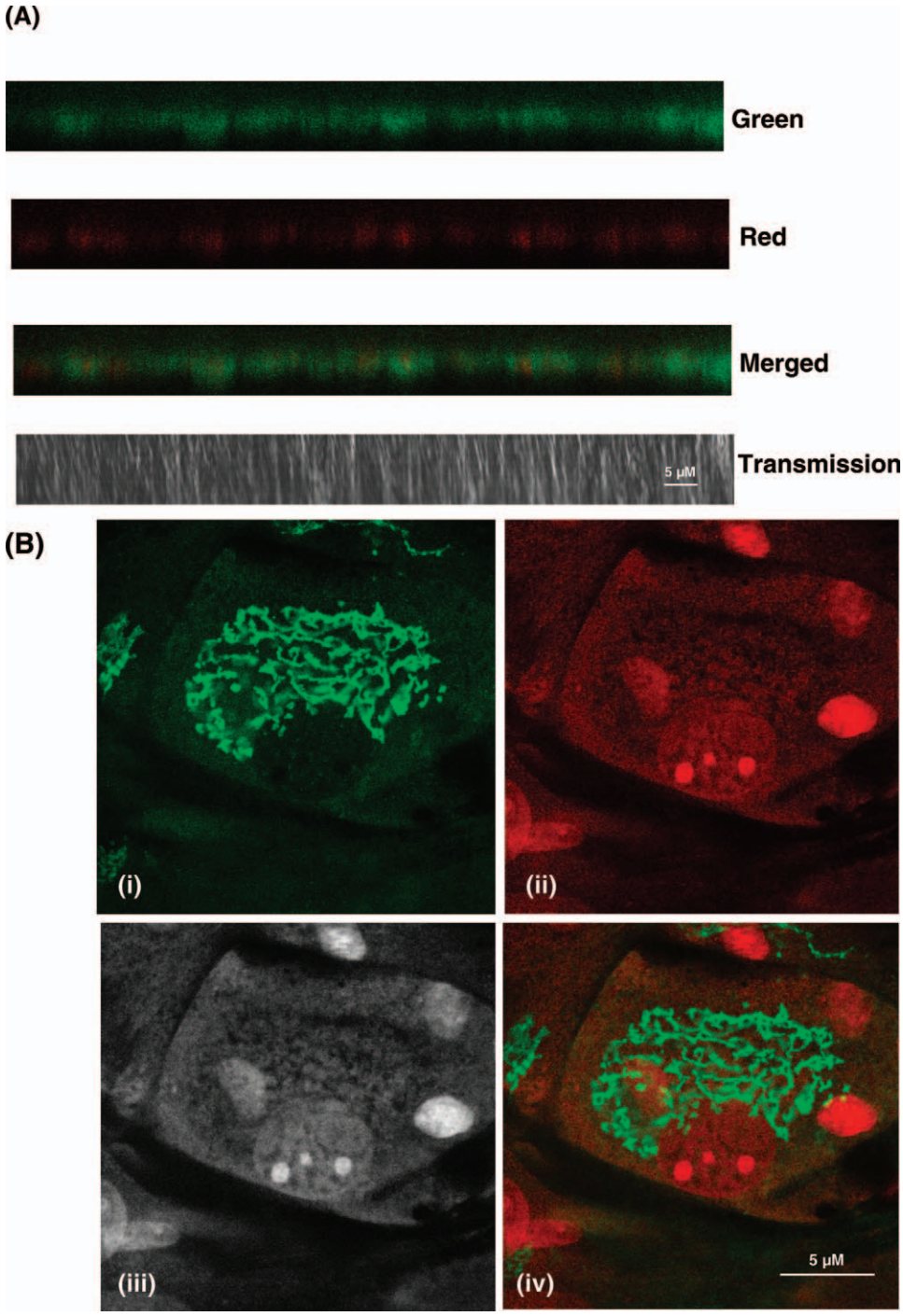

Figure 1. Presence of DMT1 and TfR in the primary choroidal epithelial cells grown in the Transwell chamber culture system. Immunostaining was conducted on the cell monolayer and examined by a confocal microscope. (A) Presence of DMT1 in cultured primary cells in vertical view. The upper side faces the medium in the inner chamber; the lower side (basolateral) of the cells rests on the permeable membrane and contacts the medium in the outer chamber. Green: DMT1 stains; red: nuclear stains. The formation of the confluent monolayer was confirmed by both merged and transmission images. (B) Presence of TfR in primary choroidal epithelial cells. i) TfR stains in green color, ii) nuclear stains in red color, iii) cell transmission image, and iv) merged staining image of TfR with nuclei. A color version of this figure is available in the online journal.

been suggested to be involved in Fe transport in the BBB (31–33). Our postulation that DMT1 mediates Fe efflux at the BCB and Mn may act on DMT1 thereby facilitating this process is supported by several evidences. First, in control cells without Mn exposure, the efflux of Fe as corrected by the leakage marker was predominant as compared to Fe influx. Mn exposure increased Fe efflux by more than 7 fold. Interestingly, by blocking the cell surface DMT1 using affinity-pure anti-DMT1 antibodies, Mn-induced elevated free Fe transport on the Transwell transport model was

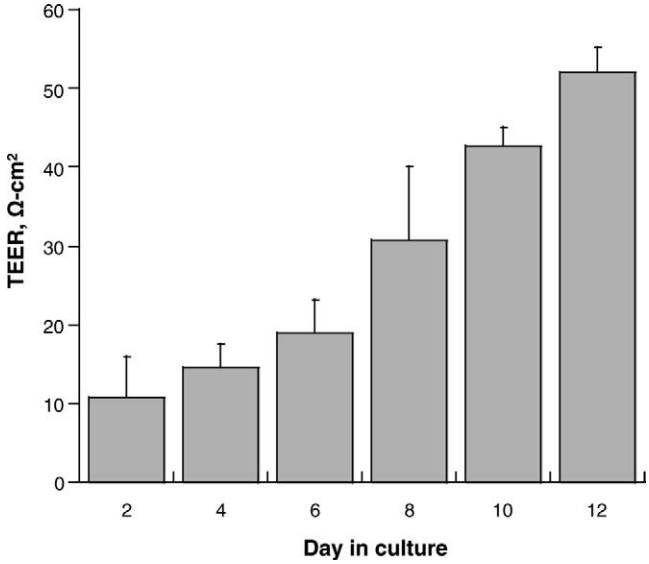

Figure 2. Transepithelial electrical resistance (TEER) values of primary choroidal epithelial cells in the BCB model. TEER values across the Transwell chamber culture system were determined every two days. TEER values increased gradually in a time-dependent manner and reached 50–60 Ω-cm^2 on day 12. Data represent mean ± SEM, $n = 3$.

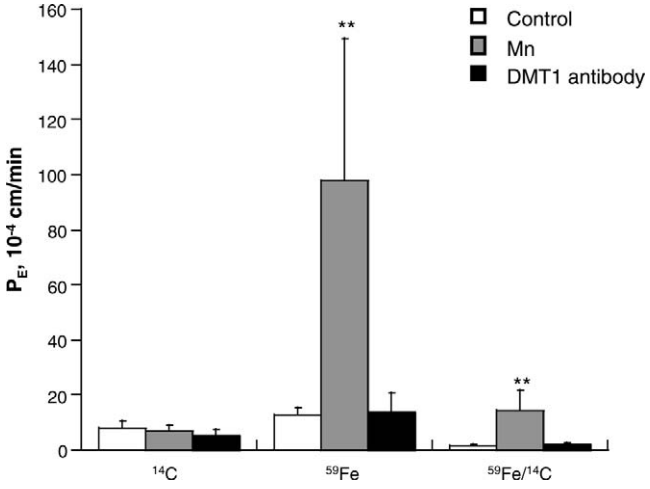

Figure 4. Fe transport in the transport model as affected by Mn exposure. Primary choroidal epithelial cells grown in the transport model were exposed to Mn (100 μM, 24 hours) prior to transport study. [^{14}C]sucrose, a space marker, was used to indicate paracellular leakage. Anti-DMT1 antibody (20 μg/ml, 2 hours) was used to block DMT1. Mn treatment significantly increased [^{59}Fe] efflux but not affecting the efflux of [^{14}C]sucrose, as compared to control. The Mn-induced increase was eliminated by the DMT1 blocking antibody. Data represent mean ± SEM, $n = 3$. ** $P < 0.01$, Mn compared to control.

completely abolished. Clearly, the anti-DMT1 antibody blocks the binding site of DMT1, thus blocking the transport of free Fe. These data support the involvement of DMT1 in the transport of free Fe by apical choroidal epithelia.

Second, the use of siRNA that specifically knocks down DMT1 makes it possible to investigate the role of DMT1 in Fe uptake and transport by the BCB. Our data demonstrated that replacement of the scrambled siRNA with the DMT1siRNA significantly reduced Fe overload as the result of Mn exposure. This observation corroborates a previous report showing that clonal DMT1 knockdown

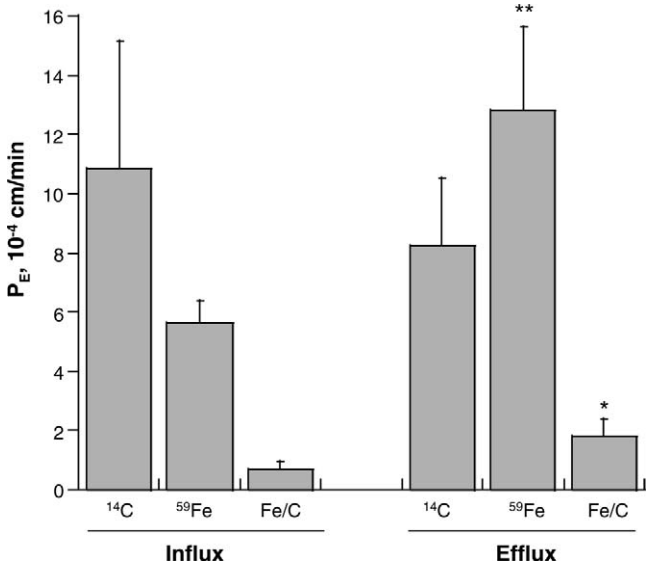

Figure 3. Comparison of influx and efflux rates of free, unbound Fe in the two-chamber Transwell transport model. The influx or efflux rate of [^{59}Fe] as determined by the P_E value was calculated from equations as described in the Materials and Methods. [^{14}C]sucrose was used to determine non-specific paracellular leakage. Fe/C was the radioactivity of [^{59}Fe] corrected by [^{14}C]sucrose. Data represent mean ± SEM, $n = 4$. ** $P < 0.01$, * $P < 0.05$, influx vs. efflux.

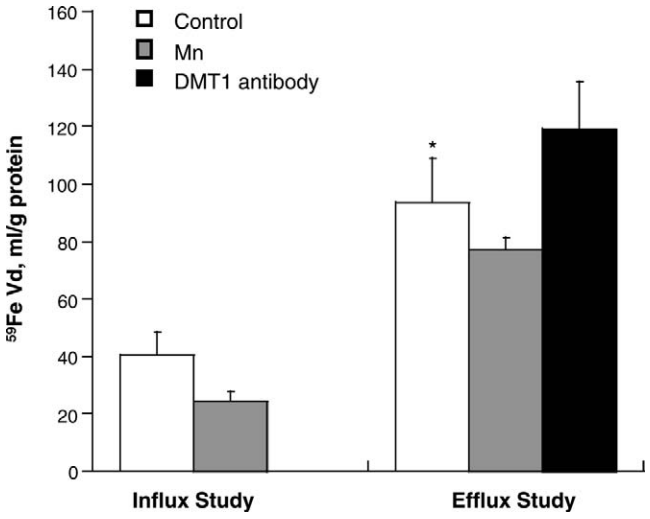

Figure 5. Fe retention in primary choroidal epithelial cells at 24 hours after Mn treatment. The assay was conducted at the end of transport study. Primary choroidal epithelial cells in the Transwell chamber were released from the membrane in cell lysis buffer. Influx Study: [^{59}Fe] was added to the outer chamber (donor). Efflux Study: [^{59}Fe] was added to the inner chamber (donor). V_d, the volume of distribution, is the ratio of tissue (dpm/g) to medium Fe concentration (dpm/mL). The antibody against DMT1 (20 μg/mL) was used to block DMT1 (2 hours, 37°C). [^{59}Fe] retention during the efflux study was significantly higher than that in the influx study. Data represent mean ± SEM, $n = 3$. * $P < 0.05$, influx vs. efflux.

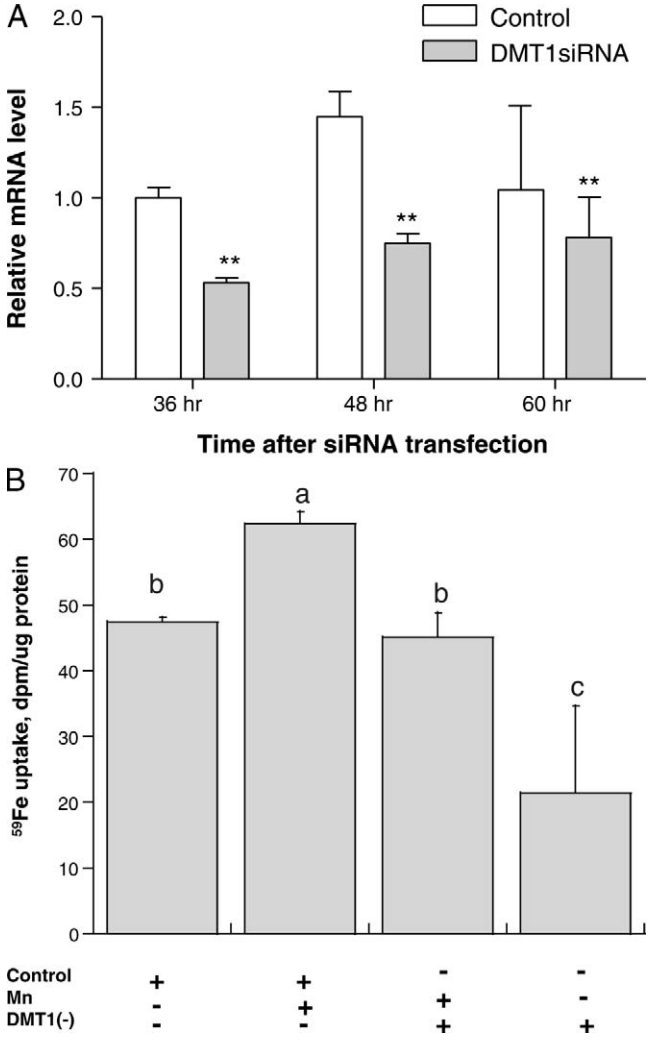

Figure 6. Fe uptake in Z310 cells following DMT1 knockdown. Choroidal epithelial Z310 cells were transfected with chemically synthesized siRNA designed for DMT1 gene knockdown. (A) Gene suppression in Z310 cells following DMT1siRNA transfection. Z310 cells were transfected with either scrambled siRNA as control or target siRNA designed to knockdown DMT1 (DMT1siRNA). Real time RT-PCR analysis revealed a significant reduction of DMT1 gene expression in DMT1siRNA group as compared to controls. Data represent mean ± SEM, $n = 4$. * $P < 0.01$, control vs. DMT1siRNA. (B) Fe uptake in DMT1 knockdown Z 310 cells. At the end of Mn exposure (100 μM, 24 hours), the cells were collected and the radioactivity was counted. Mn treatment significantly increased cellular [^{59}Fe] uptake. DMT1siRNA transfected Z310 cells were shown as DMT1 (-) and scrambled siRNA as negative control. The increased [^{59}Fe] uptake, however, was abolished after DMT1 was suppressed. Data represent mean ± SEM, $n = 3$. Bars with different letters are significantly different from one another ($P < 0.01$).

leads to a reduced Fe uptake in Caco-2 cells (34). Less uptake of Fe caused by DMT1 knockdown may also explain the decreased Fe transport across the BCB previously observed in the efflux study (Fig. 4), as a result of the pre-incubation of anti-DMT1 antibody. Our data provides direct evidence that the Mn-elicited increase in Fe efflux at the BCB is partially mediated by DMT1 although other transporter proteins, such as ZIP8, may play a role in Mn

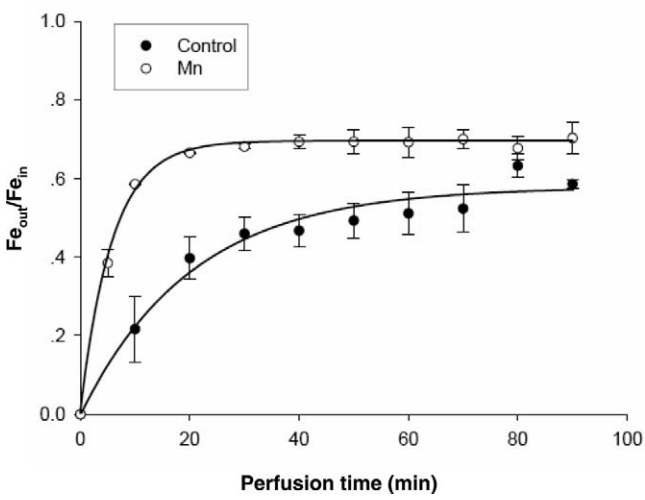

Figure 7. Effect of *in vivo* subchronic Mn exposure on Fe clearance from the CSF by *in situ* ventriculo-cisternal brain perfusion. Rats received *i.p.* injections of 6 mg Mn/kg once daily 5 days per week for 4 weeks. The artificial CSF (aCSF) containing [^{59}Fe] and [^{14}C]sucrose was infused into the lateral ventricle of rat brain and the CSF effluent was collected from the cisterna magna. Fe$_{out}$, [^{59}Fe] concentration in the collected cisternal effluent; Fe$_{in}$, [^{59}Fe] concentration in the perfusate into the lateral ventricle. The ratio of Fe$_{out}$/Fe$_{in}$ during steady-state showed a reduced Fe clearance in Mn-exposed rats than that in controls. Values are mean ± SEM, $n = 3$–4.

uptake (35). With regard to the fact that DMT1 is a hydrogen-coupled symporter, Fe uptake and transport under pH-dependent conditions deserves further exploration.

Finally, the current study provided additional *in vivo* evidence to support a role of DMT1 in mediating Fe transport at the BCB. The present result, along with our previous studies, demonstrated an over-expressed DMT1 mRNA in rat choroid plexus following subchronic exposure to Mn *in vivo*. It is known that expression of DMT1 protein is regulated by binding and unbinding of iron regulatory

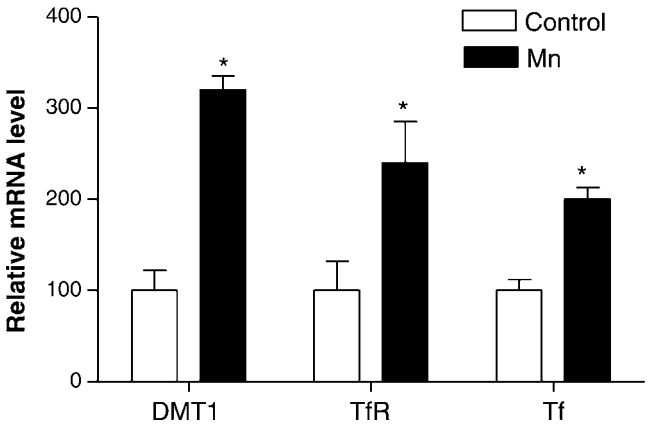

Figure 8. Expression of DMT1, TfR and Tf mRNA in rat choroid plexus as affected by subchronic Mn exposure. $MnCl_2$ was administrated by *i.p.* injection to rats at a dose of 6 mg of Mn/kg for 4 consecutive weeks. The relative mRNA levels of DMT1, TfR, Tf and β-actin were quantified by real-time RT-PCR and expressed as the ratio of DMT1/β-actin, TfR/β-actin or Tf/β-actin. Data represent mean ± SEM, $n = 3$; * $P < 0.05$, as compared to control.

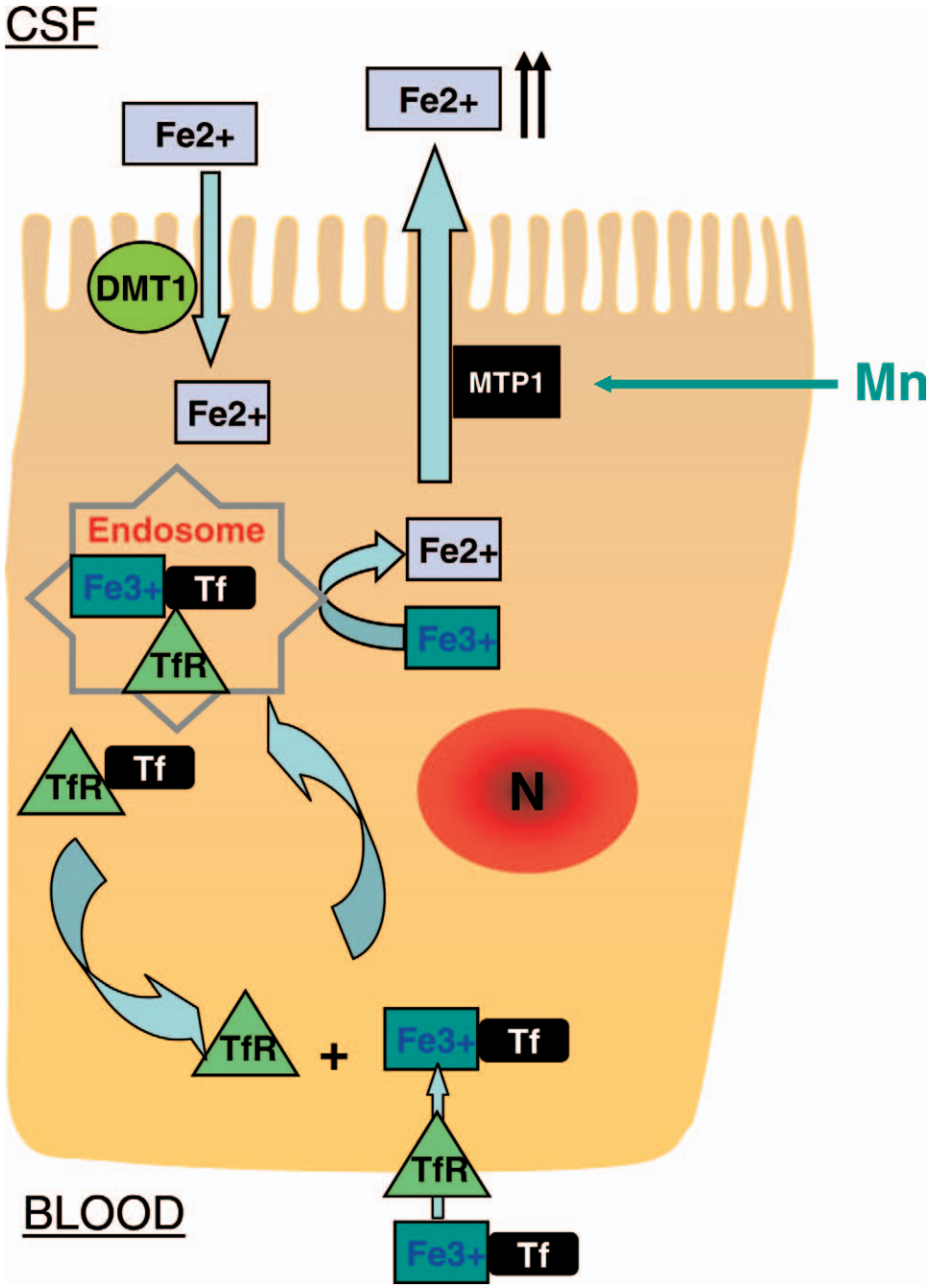

Figure 9. Proposed mechanism of Fe transport at the BCB. Fe in the blood, as Tf-bound Fe^{3+}, is transported by a TfR-mediated endocytosis across the basolateral membrane into the choroidal epithelial cells. Within endosomes, ferric Fe is reduced to ferrous Fe by oxidoreductase. Cellular Fe is then bound to ferroportin or MTP1, which functions to expel Fe into the CSF. In the opposite direction, free Fe in the CSF is taken up by DMT1 located in the apical membrane of the choroidal epithelial cell. In the Transwell model and under the normal condition, the DMT1-mediated Fe uptake at apical membrane may surpass the TfR-mediated transport from the basolateral side, serving as the normal process for Fe clearance in the CSF. Mn exposure *in vitro*, by increasing DMT1 expression, appears to facilitate the "efflux" of Fe from the CSF to the blood. However, under the *in vivo* condition, Mn exposure translocates MTP1 toward the apical microvilli of the choroid plexus (22) and activates the MTP1-mediated process to expel excess intracellular Fe toward apical CSF compartment. This process may offset DMT1-mediated Fe uptake on the apical membrane. The net *in vivo* result is a diminished Fe clearance by the choroid plexus and an increased Fe in the CSF. TfR, transferrin receptor; N, nucleus. A color version of this figure is available in the online journal.

protein-1 (IRP1) to the stem-loop structures in DMT1 mRNA (10). Our previous studies have also shown that Mn exposure may replace a forth liable Fe in [Fe-S] cluster of IRP1, making it more stable in binding to DMT1 mRNA and leading to over-expression of DMT1 protein (12). As DMT1 molecules are primarily concentrated within the apical microvilli and toward the apical membrane (22), it therefore makes sense that DMT1 may mediate Fe uptake

into the choroidal epithelial cells through the apical microvilli.

Why, then, did *in vivo* Mn exposure reduce Fe clearance from the CSF by the choroid plexus in the face of increased efflux of Fe as seen *in vitro*? One should keep in mind that both TfR and DMT1 coordinately regulate Fe transport at the blood and CSF interface and both of their protein expressions can be altered by Mn exposure. In Belgrade rats defective in DMT1, non-Tf-bound transport is diminished. Interestingly, Tf-mediated Fe uptake is also altered, indicating that DMT1 may coordinate with TfR to mediate Fe transport by participating in the release of Fe from endosome (36, 37). Consistent with our previous reports (9–12), the current study found an over-expressed TfR in the choroid plexus as a result of subchronic Mn exposure. In intact animal, it is possible that Tf-bound Fe may be delivered to choroidal epithelial cells through receptor-mediated internalization localized in basal lateral side of the BCB facing the blood compartment. Within the cells in acidic endosomal compartment, Fe ions are released in the form of free Fe, which become the substrates of another nonspecific Fe transport protein, ferroportin or metal transport protein-1 (MTP1) (Fig. 9). Unlike DMT1, ferroportin functions to expel metals from the cytosol to extracellular space (38–40). Our recent evidence has clearly shown that upon Mn treatment, ferroportin proteins are visibly translocated to apical microvilli of the choroid plexus and function to transport intracellular Fe toward the CSF (22).

In the opposite direction, non-Tf bound, free Fe in the CSF may gain access to the choroid plexus via the apical DMT1 as observed in the current *in vitro* experiments. Presumably, DMT1-mediated efflux would offset TfR-mediated influx based on the current two-chamber Transwell data. However, the cellular overload of Fe *in vivo* following Mn exposure may activate the ferroportin-mediated processes (22), which would expel excess Fe from the choroidal epithelial cells, unidirectionally, to the CSF. Thus, the net result of the choroid plexus in clearing excess Fe in the CSF would seem likely to diminish, as demonstrated in our *in situ* ventriculo-cisternal perfusion study performed in Mn-exposed rats. Thus, the ultimate outcome following subchronic Mn exposure *in vivo* is the increased Fe concentration in the CSF (Fig. 9).

Clinically, increased Fe levels in the brain have been demonstrated in numerous neurodegenerative diseases, owing to intracellular Fe imbalance associated with either increased Fe uptake or decreased Fe release (41). High Fe contents have been found in the brains of Alzheimer's patients accompanying the alteration of the expression in other Fe transport related proteins, such as ferritin, transferrin and TfR. These are also seen in basal ganglia and substantia nigra of Parkinsonian patients' brain (42). A number of studies have shown that Mn-initiated neurotoxicity is associated with Fe dysregulation. In the welders exposed to long-term, low-levels of Mn, altered Fe concentration has been demonstrated (43–45). High Mn in the diet increases Fe uptake into rat brain (46) and similarly Fe uptake is also increased in the cultured choroidal epithelial Z310 cells after Mn treatment (10, 46). The Mn-facilitated Fe transport across the BCB, as demonstrated in the current study, may be largely responsible for the disrupted Fe homeostasis in brain through altered expression of transporter proteins at the BCB. Furthermore, Fe-initiated oxidative stress through Fenton reaction has been demonstrated in the welders exposed to airborne Mn (47).

In summary, by using a primary rat choroidal epithelial Transwell model system, we demonstrated that free, unbound Fe species were transported by the blood-CSF barrier favorably from the CSF to blood via a DMT1-mediated transport mechanism; Mn exposure, *in vitro*, may facilitate the efflux of Fe from the CSF to the blood. However, following *in vivo* subchronic exposure to Mn, the clearance of Fe from the CSF by the choroid plexus was greatly reduced. Enhanced TfR-mediated influx of Fe from the blood to the CSF and intracellular relocation of ferroportin to expel Fe toward the CSF may compromise DMT1-mediated efflux, leading to an increased Fe concentration in the CSF.

We gratefully acknowledge Dr. Yanshu Zhang for her assistance in the ventriculo-cisternal brain perfusion and Dr. Janelle S. Crossgrove for her assistance in primary culture for rat choroidal epithelia.

1. Zheng W, Aschner M, Ghersi-Egea JF. Brain barrier systems: a new frontier in metal neurotoxicological research. Toxicol Appl Pharmacol 192:1–11, 2003.
2. Jellinger KA. The role of iron in neurodegeneration: prospects for pharmacotherapy of Parkinson's disease. Drugs Aging 14:115–140, 1999.
3. Holtz WA, Turetzky JM, Jong YJ, O'Malley KL. Oxidative stress-triggered unfolded protein response is upstream of intrinsic cell death evoked by parkinsonian mimetics. J Neurochem 99:54–69, 2006.
4. Shinde S, Pasupathy K. Respiratory-chain enzyme activities in isolated mitochondria of lymphocytes from patients with Parkinson's disease: preliminary study. Neurol India 54:390–393, 2006.
5. Szeto HH. Mitochondria-targeted peptide antioxidants: novel neuroprotective agents. Aaps J 8:E521–531, 2006.
6. Moos T. Immunohistochemical localization of intraneuronal transferrin receptor immunoreactivity in the adult mouse central nervous system. J Comp Neurol 375:675–692, 1996.
7. Berg D, Gerlach M, Youdim MB, Double KL, Zecca L, Riederer P, Becker G. Brain iron pathways and their relevance to Parkinson's disease. J Neurochem 79:225–236, 2001.
8. Zheng W, Zhao Q, Slavkovich V, Aschner M, Graziano JH. Alteration of iron homeostasis following chronic exposure to manganese in rats. Brain Res 833:125–132, 1999.
9. Li GJ, Choi BS, Wang X, Liu J, Waalkes MP, Zheng W. Molecular mechanism of distorted iron regulation in the blood-CSF barrier and regional blood-brain barrier following in vivo subchronic manganese exposure. Neurotoxicology 27:737–744, 2006.
10. Zheng W, Zhao Q. Iron overload following manganese exposure in cultured neuronal, but not neuroglial cells. Brain Res 897:175–179, 2001.
11. Li GJ, Zhao Q, Zheng W. Alteration at translational but not

transcriptional level of transferrin receptor expression following manganese exposure at the blood-CSF barrier in vitro. Toxicol Appl Pharmacol 205:188–200, 2005.
12. Wang X, Li GJ, Zheng W. Upregulation of DMT1 expression in choroidal epithelia of the blood-CSF barrier following manganese exposure in vitro. Brain Res 1097:1–10, 2006.
13. Bradbury MW. Transport of iron in the blood-brain-cerebrospinal fluid system. J Neurochem 69:443–454, 1997.
14. Moos T, Morgan EH. Evidence for low molecular weight, non-transferrin-bound iron in rat brain and cerebrospinal fluid. J Neurosci Res 54:486–494, 1998.
15. Ueda F, Raja KB, Simpson RJ, Trowbridge IS, Bradbury MW. Rate of 59Fe uptake into brain and cerebrospinal fluid and the influence thereon of antibodies against the transferrin receptor. J Neurochem 60:106–113, 1993.
16. Deane R, Zheng W, Zlokovic BV. Brain capillary endothelium and choroid plexus epithelium regulate transport of transferrin-bound and free iron into the rat brain. J Neurochem 88:813–820, 2004.
17. Li CY, Watkins JA, Glass J. The H(+)-ATPase from reticulocyte endosomes reconstituted into liposomes acts as an iron transporter. J Biol Chem 269:10242–10246, 1994.
18. Gunshin H, Mackenzie B, Berger UV, Gunshin Y, Romero MF, Boron WF, Nussberger S, Gollan JL, Hediger MA. Cloning and characterization of a mammalian proton-coupled metal-ion transporter. Nature 388:482–488, 1997.
19. Tabuchi M, Tanaka N, Nishida-Kitayama J, Ohno H, Kishi F. Alternative splicing regulates the subcellular localization of divalent metal transporter 1 isoforms. Mol Biol Cell 13:4371–4387, 2002.
20. Qian ZM, Shen X. Brain iron transport and neurodegeneration. Trends Mol Med 7:103–108, 2001.
21. Hentze MW, Muckenthaler MU, Andrews NC. Balancing acts: molecular control of mammalian iron metabolism. Cell 117:285–297, 2004.
22. Wang X, Miller DS, Zheng W. Intracellular trafficking of metal transporters in intact rat choroid plexus following in vitro treatment of manganese or iron. Toxicol Appl Pharmacol (in press).
23. Zheng W, Zhao Q, Graziano JH. Primary culture of choroidal epithelial cells: characterization of an in vitro model of blood-CSF barrier. In Vitro Cell Dev Biol Anim 34:40–45, 1998.
24. Zheng W, Zhao Q. The blood-CSF barrier in culture. Development of a primary culture and transepithelial transport model from choroidal epithelial cells. Methods Mol Biol 188:99–114, 2002.
25. Zheng W, Zhao Q. Establishment and characterization of an immortalized Z310 choroidal epithelial cell line from murine choroid plexus. Brain Res 958:371–380, 2002.
26. Shi LZ, Zheng W. Establishment of an in vitro brain barrier epithelial transport system for pharmacological and toxicological study. Brain Res 1057:37–48, 2005.
27. Al-Sarraf H, Philip L. Effect of hypertension on the integrity of blood brain and blood CSF barriers, cerebral blood flow and CSF secretion in the rat. Brain Res 975:179–188, 2003.
28. Al-Sarraf H, Philip L. Increased brain uptake and CSF clearance of 14C-glutamate in spontaneously hypertensive rats. Brain Res 994:181–187, 2003.
29. Strazielle N, Ghersi-Egea JF. Demonstration of a coupled metabolism-efflux process at the choroid plexus as a mechanism of brain protection toward xenobiotics. J Neurosci 19:6275–6289, 1999.
30. Crossgrove JS, Li GJ, Zheng W. The choroid plexus removes beta-amyloid from brain cerebrospinal fluid. Exp Biol Med (Maywood) 230: 771–776, 2005.
31. Faucheux BA, Nillesse N, Damier P, Spik G, Mouatt-Prigent A, Pierce A, Leveugle B, Kubis N, Hauw JJ, Agid Y. Expression of lactoferrin receptors is increased in the mesencephalon of patients with Parkinson disease. Proc Natl Acad Sci U S A 92:9603–9607, 1995.
32. Qian ZM, Wang Q. Expression of iron transport proteins and excessive iron accumulation in the brain in neurodegenerative disorders. Brain Res Brain Res Rev 27:257–267, 1998.
33. Malecki EA, Devenyi AG, Beard JL, Connor JR. Existing and emerging mechanisms for transport of iron and manganese to the brain. J Neurosci Res 56:113–122, 1999.
34. Bannon DI, Abounader R, Lees PS, Bressler JP. Effect of DMT1 knockdown on iron, cadmium, and lead uptake in Caco-2 cells. Am J Physiol Cell Physiol 284:C44–50, 2003.
35. He L, Girijashanker K, Dalton TP, Reed J, Li H, Soleimani M, Nebert DW. ZIP8, member of the solute-carrier-39 (SLC39) metal-transporter family: characterization of transporter properties. Mol Pharmacol 70: 171–180, 2006.
36. Oates PS, Morgan EH. Defective iron uptake by the duodenum of Belgrade rats fed diets of different iron contents. Am J Physiol 270: G826–832, 1996.
37. Garrick LM, Dolan KG, Romano MA, Garrick MD. Non-transferrin-bound iron uptake in Belgrade and normal rat erythroid cells. J Cell Physiol 178:349–358, 1999.
38. Donovan A, Brownlie A, Zhou Y, Shepard J, Pratt SJ, Moynihan J, Paw BH, Drejer A, Barut B, Zapata A, Law TC, Brugnara C, Lux SE, Pinkus GS, Pinkus JL, Kingsley PD, Palis J, Fleming MD, Andrews NC, Zon LI. Positional cloning of zebrafish ferroportin1 identifies a conserved vertebrate iron exporter. Nature 403:776–781, 2000.
39. McKie AT, Marciani P, Rolfs A, Brennan K, Wehr K, Barrow D, Miret S, Bomford A, Peters TJ, Farzaneh F, Hediger MA, Hentze MW, Simpson RJ. A novel duodenal iron-regulated transporter, IREG1, implicated in the basolateral transfer of iron to the circulation. Mol Cell 5:299–309, 2000.
40. Wu LJ, Leenders AG, Cooperman S, Meyron-Holtz E, Smith S, Land W, Tsai RY, Berger UV, Sheng ZH, Rouault TA. Expression of the iron transporter ferroportin in synaptic vesicles and the blood-brain barrier. Brain Res 1001:108–117, 2004.
41. Aisen P, Wessling-Resnick M, Leibold EA. Iron metabolism. Curr Opin Chem Biol 3:200–206, 1999.
42. Thompson KJ, Shoham S, Connor JR. Iron and neurodegenerative disorders. Brain Res Bull 55:155–164, 2001.
43. Ellingsen DG, Haug E, Ulvik RJ, Thomassen Y. Iron status in manganese alloy production workers. J Appl Toxicol 23:239–247, 2003.
44. Powers KM, Smith-Weller T, Franklin GM, Longstreth WT, Swanson PD, Checkoway H. Parkinson's disease risks associated with dietary iron, manganese, and other nutrient intakes. Neurology 60:1761–1766, 2003.
45. Lu L, Zhang LL, Li GJ, Guo W, Liang W, Zheng W. Alteration of serum concentrations of manganese, iron, ferritin, and transferrin receptor following exposure to welding fumes among career welders. Neurotoxicology 26:257–265, 2005.
46. Chua AC, Morgan EH. Effects of iron deficiency and iron overload on manganese uptake and deposition in the brain and other organs of the rat. Biol Trace Elem Res 55:39–54, 1996.
47. Li GJ, Zhang LL, Lu L, Wu P, Zheng W. Occupational exposure to welding fume among welders: alterations of manganese, iron, zinc, copper, and lead in body fluids and the oxidative stress status. J Occup Environ Med 46:241–248, 2004.